Numerical Simulation of Pulse-Tube Refrigerators: 1D model

I.A. Lyulina[1], R.M.M. Mattheij[1], A.S. Tijsseling[1], A.T.A.M. de Waele[2]

[1]Department of Mathematics and Computer Science, [2]Department of Applied Physics
Eindhoven University of Technology, PO Box 513, 5600 MB Eindhoven, The Netherlands

Abstract A new numerical model has been introduced to study steady oscillatory heat and mass transfer in the tube section of a pulse-tube refrigerator. Conservation equations describing compressible gas flow in the tube are solved numerically, using high resolution schemes. The equation of conservation of momentum is neglected because the pressure is justified to be uniform in space. The model reduces to solving the equations of conservation of mass and energy. Using our numerical model, we can study the temperature dynamics in the pulse tube, calculate the average enthalpy flow and estimate the refrigeration power.

Keywords: pulse-tube refrigerator, numerical simulation, high resolution scheme

1 Introduction

The pulse tube is a relatively new type of refrigerator. It was introduced in the early sixties. At that time the pulse tube was abandoned as a useful cooler because of its inefficiency. The performance of these devices, today known as basic pulse tubes was limited, typically reaching temperatures of about 120 K. A significant improvement was made in 1984 by Mikulin [1], who introduced the orifice pulse tube. Due to this modification the performance of pulse tubes increased and for the first time it became comparable to the performance of practical coolers (Stirling cycle, Gifford-McMahon and Joule-Thomson cryocoolers). Since then the improvement in efficiency and in performance went fast. By the end of 1990s, temperatures below 2K had been reached [2].

The development of pulse-tube cryocoolers is still at an early stage. Only few models are currently in production. However, pulse-tube cryocoolers are beginning to replace the older types of cryocoolers in a wide variety of military, aerospace, industrial and medical applications. Advantages such as simplicity, low cost and reliability, combined with high performance, have resulted in an extensive study of pulse tubes in recent years.

To predict the performance and optimise the operational conditions, various analytical and numerical models have been developed. Thermodynamical models [3], [4] use the laws of thermodynamics to analyse the performance of the pulse tube. Such models are important for understanding the physical processes occurring in the pulse tube. General relations between thermodynamical quantities can be derived. However, for the accurate prediction of pulse tube performance, one has to analyse compressible oscillating gas flow using fluid dynamics. Due to the non-linearity of the conservation equations, analytical solutions are essentially impossible. This is why numerical models are of great importance. One of the earliest papers on numerical modelling of the orifice pulse tubes was [5]. The one-dimensional system of conservation equations was solved using the finite volume method. Several papers with two-dimensional modelling have appeared recently, see [6, 7, 8]. In [9] results of three-dimensional computations are presented. These were obtained using commercially available CFX package. Three-dimensional modelling appears to be time consuming and therefore has not been applicable for real system optimisation until now. In this paper we base our numerical simulations on a different mathematical model introduced in [10]. According to our approach the equation for conservation of momentum can be neglected as the pressure is considered to be uniform in space. The
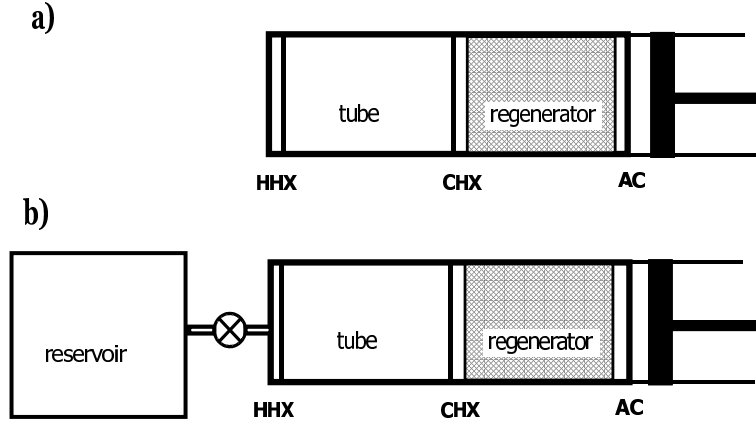
Figure 1: A schematic picture of the Stirling-type pulse-tube refrigerators :(a) the basic pulse tube and (b) the orifice pulse tube. From right to left the basic system consists of a piston, an aftercooler (AC), a regenerator, a cold heat exchanger (CHX), a tube, a hot heat exchanger (HHX). In (b) the system is extended with an orifice and a reservoir (buffer).

model is then based on the conservation of mass and energy equations. We validate this approach by comparing our results with results from three-dimensional [9] and harmonic [4] modelling. The main benefits of our model are that it is not computationally expensive (as full three-dimensional models) and that it is not restricted to the harmonic time dependence (as harmonic models).

The paper is built up as follows. The physical model is described in section 2. The mathematical model is introduced and non-dimensionalised in Section 3. In the end of this section a reduced system suitable for numerical solution is discussed. In Section 4, numerical methods for solving equations for temperature and velocity are explained. In Section 5, the results of our computations are presented. Temperature, mass flow and enthalpy flow for two different pressure variations are presented. Section 6 summarizes the main results and proposes future work.

2   Physical model

The essential elements of a pulse-tube refrigerator are shown in Fig. 1. The pulse tube works by the cyclic compression and expansion of a gas, usually helium. Due to heat exchange between gas, regenerator, tube walls and the two heat exchangers, a temperature difference arises along the tube. The pressure oscillations in the system are generated by a piston compressor or ,alternatively, by switching valves. The aftercooler (AC), see Fig. 1a, removes the heat of compression so that the regenerator can work more efficiently. The regenerator acts as a buffer: it absorbs heat from the gas on the compression part of the pressure cycle and it returns heat to the gas on the expansion part. To achieve this, the regenerator is filled with a matrix - some kind of solid material with a large heat capacity and a large heat exchanging surface. The cold heat exchanger (CHX) is the coldest point of the system. Here the heat is extracted from the load to be cooled. In the tube, the compressible gas oscillates. If there is a suitable phase relationship between the pressure and the gas flow, heat will be transported from the cold end to the warm end. The hot heat exchanger (HHX) removes the heat carried through the tube. The hot heat exchanger is maintained at ambient temperature. In the orifice design, see Fig. 1b, the basic pulse tube is modified by adding a reservoir and an orifice. The reservoir is large compared to the pulse tube volume so that the pressure inside is approximately constant. Gas flows through the orifice due to a pressure difference. More gas is contributing now to the cooling power and this improves the efficiency of the cooler.

Fig. 2 shows the energy flow in the pulse tube. At the hot heat exchanger heat $\dot{Q}_H$ is extracted from the system. At the cold heat exchanger heat $\dot{Q}_C$ is put in to the system. There is a net enthalpy flow from the cold heat exchanger to the hot heat exchanger. According to the first law of thermodynamics the average cooling power is equal to the enthalpy flow in the pulse tube. As to study the energy transfer from the cold to the hot end we will concentrate solely on the tube section of the pulse-tube refrigerator.
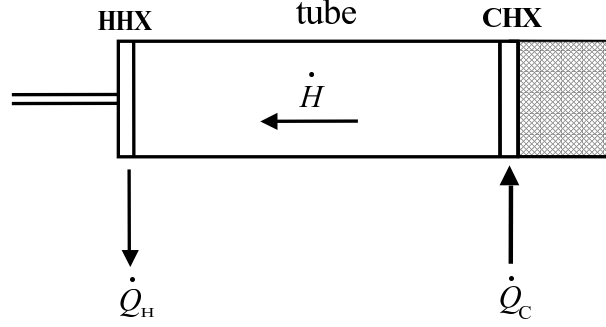
Figure 2: Net heat and enthalpy flows in the tube.

3 Mathematical model

3.1 Governing equations

We consider a one-dimensional region $0 < x < L$, where L is the length of the tube section of the cooler. We assume that the fluid is Newtonian, the gas is ideal and the flow is laminar. Let us denote the density by $\rho(x,t)$, the velocity by $u(x,t)$, the temperature by $T(x,t)$, the pressure by $p(x,t)$, the dynamic viscosity by μ, the specific heat capacity of the gas at constant pressure by c_p, the thermal conductivity of the gas by k_g and the specific ideal gas constant by R_m. The equations for mass, momentum and energy conservation and the equation of state are

$$\frac{\partial \rho}{\partial t} + \frac{\partial}{\partial x}(\rho u) = 0, \tag{1}$$

$$\rho\left(\frac{\partial u}{\partial t} + u\frac{\partial u}{\partial x}\right) = -\frac{\partial p}{\partial x} + \frac{4}{3}\frac{\partial}{\partial x}\left(\mu\frac{\partial u}{\partial x}\right), \tag{2}$$

$$\rho c_p\left(\frac{\partial T}{\partial t} + u\frac{\partial T}{\partial x}\right) = \frac{\partial p}{\partial t} + u\frac{\partial p}{\partial x} + \frac{\partial}{\partial x}\left(k_g\frac{\partial T}{\partial x}\right), \tag{3}$$

$$p = \rho R_m T. \tag{4}$$

Quasi-steady wall friction, which would give an additional term $-32\mu u/D^2$ (D is the tube diameter) in the momentum equation is considered to be part of two-dimensional modelling. To complete the system we need initial and boundary conditions. These will be given in Section 3.3.

3.2 Non-dimensionalisation

The system of equations (1)-(4) will first be made dimensionless. The scaling parameters are chosen as follows: the shortest physical time-scale of importance is $1/\omega$ (time for one piston oscillation multiplied by 2π), where ω is the angular frequency of the piston movement. We introduce $\bar{u}$ to be a representative value for the velocity and therefore $\bar{u}/\omega$ to be a typical length-scale. Let $\bar{p}$ be the amplitude of the pressure oscillations, p_b the buffer pressure, T_a an ambient temperature, $\bar{\rho}$ a typical density, $\bar{\mu}$ a typical viscosity and $\bar{k}_g$ a typical thermal conductivity of the gas. We take the pressure variation caused by the piston or valves to be $p_p(t) = p_0 + \bar{p}\hat{p}(t)$, where $\hat{p}(t)$ is a known function of time. We introduce dimensionless variables (indicated by a hat) via

$$\begin{aligned}
\rho = \bar{\rho}\hat{\rho}, \quad T = T_a\hat{T}, \quad p = p_0 + \bar{p}\hat{p}, \quad u = \bar{u}\hat{u}, \\
x = (\bar{u}/\omega)\hat{x}, \quad t = \hat{t}/\omega, \quad \mu = \bar{\mu}\hat{u}, \quad k_g = \bar{k}_g\hat{k}_g.
\end{aligned} \tag{5}$$

The governing equations (1)-(4) become (without ambiguity the hats on the dimensionless variables can be omitted):

$$\frac{\partial \rho}{\partial t} + \frac{\partial}{\partial x}(\rho u) = 0, \tag{6}$$

3

$$\rho \left(\frac{\partial u}{\partial t} + u \frac{\partial u}{\partial x} \right) = -\frac{1}{\mathrm{Ma}^2} \frac{\partial p}{\partial x} + \frac{4}{3\mathrm{Re}} \frac{\partial}{\partial x} \left(\mu \frac{\partial u}{\partial x} \right), \tag{7}$$

$$\rho \left(\frac{\partial T}{\partial t} + u \frac{\partial T}{\partial x} \right) = \frac{\mathrm{Ec}}{\mathrm{Ma}^2} \left(\frac{\partial p}{\partial t} + u \frac{\partial p}{\partial x} \right) + \frac{1}{\mathrm{Pe}} \frac{\partial}{\partial x} \left(k_g \frac{\partial T}{\partial x} \right), \tag{8}$$

$$(\mathcal{A} + p)\mathcal{B} = \rho T. \tag{9}$$

In our simulations we consider the pulse tube operating at 20Hz. For such tubes the typical velocity is 1.5 m/s. The average distance which gas particles travel in the tube (displacement length) is 0.012m. The length of the tube is 0.2 m. All necessary physical data for a typical single-inlet pulse tube are given in Table 1. The relevant dimensionless numbers are

$$Reynolds \quad number \quad \mathrm{Re} = \frac{\bar{\rho}\bar{u}^2}{\bar{\mu}\omega} \sim 4 \times 10^3,$$

$$Prandtl \quad number \quad \mathrm{Pr} = \frac{c_p \bar{\mu}}{\bar{k}_g} \sim 0.658,$$

$$Peclet \quad number \quad \mathrm{Pe} = \mathrm{RePr} = \frac{\bar{\rho}\bar{u}^2 c_p}{\omega \bar{k}_g} \sim 2.6 \times 10^3,$$

$$Mach \quad number \quad \mathrm{Ma} = \frac{\bar{u}}{(\bar{p}/\bar{\rho})^{1/2}} \sim 4.6 \times 10^{-3},$$

$$Eckert \quad number \quad \mathrm{Ec} = \frac{\bar{u}^2}{c_p T_a} \sim 4.5 \times 10^{-6}.$$

The unsteady Reynolds number indicates how strong the inertia is with respect to the viscous effects. The Prandtl number gives an indication for the diffusivity of heat with respect to the diffusivity of momentum. Pr only depends on the properties of the fluid. The Peclet number shows the ratio of advection of heat to the conduction of heat. The Mach number characterizes the compressibility of flow. The Eckert number gives the kinetic energy against thermal energy.

The considerations above show that the basic equations (6)-(9) contain six dimentionless parameters: $1/\mathrm{Ma}^2$, $1/\mathrm{Re}$, $\mathrm{Ec}/\mathrm{Ma}^2$, $1/\mathrm{Pe}$, $\mathcal{A}$ and $\mathcal{B}$. Typical values are given in Table 2.

3.3 Simplified system

The momentum equation (7) can be rewritten as follows

$$\frac{\partial p}{\partial x} = \frac{4\mathrm{Ma}^2}{3\mathrm{Re}} \frac{\partial}{\partial x} \left(\mu \frac{\partial u}{\partial x} \right) - \mathrm{Ma}^2 \rho \left(\frac{\partial u}{\partial t} + u \frac{\partial u}{\partial x} \right). \tag{10}$$

The first and second terms on the right hand side represent viscous and inertial forces. Dimensional analysis reveals that the constants $\mathrm{Ma}^2/\mathrm{Re}$ and Ma^2 are the order of 10^{-9} and 10^{-5}, respectively. This means that the inertial and viscous forces are too small to produce a significant pressure gradient; so the right-hand side of equation (10) is approximately zero. Therefore the pressure is uniform in space and the momentum equation can be neglected. The system (6)-(9) now simplifies to:

$$\frac{\partial \rho}{\partial t} + \frac{\partial}{\partial x}(\rho u) = 0, \tag{11}$$

$$\frac{\partial p}{\partial x} = 0, \tag{12}$$

$$\rho \left(\frac{\partial T}{\partial t} + u \frac{\partial T}{\partial x} \right) = \frac{\mathrm{Ec}}{\mathrm{Ma}^2} \frac{dp}{dt} + \frac{1}{\mathrm{Pe}} \frac{\partial}{\partial x} \left(k_g \frac{\partial T}{\partial x} \right), \tag{13}$$

4

$$(\mathcal{A} + p(t))\mathcal{B} = \rho T. \tag{14}$$

Combining the equations (11) and (13) we derive:

$$\frac{\partial(\rho T)}{\partial t} + \frac{\partial(\rho u T)}{\partial x} = \frac{\mathrm{Ec}}{\mathrm{Ma}^2}\frac{dp}{dt} + \frac{1}{\mathrm{Pe}}\frac{\partial}{\partial x}\left(k_g \frac{\partial T}{\partial x}\right). \tag{15}$$

Now we substitute (14) in the left-hand side of (15):

$$\frac{d((\mathcal{A} + p(t))\mathcal{B})}{dt} + \frac{\partial((\mathcal{A} + p(t))\mathcal{B}u)}{\partial x} = \frac{\mathrm{Ec}}{\mathrm{Ma}^2}\frac{dp}{dt} + \frac{1}{\mathrm{Pe}}\frac{\partial}{\partial x}\left(k_g \frac{\partial T}{\partial x}\right). \tag{16}$$

We thus find the following equation for the velocity:

$$\frac{\partial u}{\partial x} = (\frac{\mathrm{Ec}}{\mathrm{Ma}^2} - \mathcal{B})\frac{1}{\mathcal{B}(\mathcal{A}+p(t))}\frac{dp}{dt} + \frac{1}{\mathcal{B}(\mathcal{A}+p(t))}\frac{1}{\mathrm{Pe}}\frac{\partial}{\partial x}\left(k_g \frac{\partial T}{\partial x}\right). \tag{17}$$

In order to obtain the equation for the temperature, we eliminate the density in (8), using equation (9). Finally the equations for the velocity and temperature are

$$\frac{\partial u}{\partial x} = \epsilon\frac{\partial}{\partial x}\left(k_g \frac{\partial T}{\partial x}\right) + s_1(t), \tag{18}$$

$$\frac{\partial T}{\partial t} = \epsilon T\frac{\partial}{\partial x}\left(k_g \frac{\partial T}{\partial x}\right) - u\frac{\partial T}{\partial x} + s_2(t)T, \tag{19}$$

where

$$s_1(t) = (\frac{\mathrm{Ec}}{\mathrm{Ma}^2} - \mathcal{B})\frac{1}{\mathcal{B}(\mathcal{A}+p(t))}\frac{dp}{dt}, \tag{20}$$

$$s_2(t) = \frac{\mathrm{Ec}}{\mathrm{Ma}^2}\frac{1}{\mathcal{B}(\mathcal{A}+p(t))}\frac{dp}{dt}, \tag{21}$$

$$\epsilon = \frac{1}{\mathcal{B}(\mathcal{A}+p(t))}\frac{1}{\mathrm{Pe}} \ll 1. \tag{22}$$

Assuming that the gas thermal conductivity k_g is constant the equations (18), (19) can be simplified:

$$\frac{\partial u}{\partial x} = \epsilon\frac{\partial^2 T}{\partial x^2} + s_1(t), \tag{23}$$

$$\frac{\partial T}{\partial t} = \epsilon T\frac{\partial^2 T}{\partial x^2} - u\frac{\partial T}{\partial x} + s_2(t)T. \tag{24}$$

The temperature equation (24) is a nonlinear convection-diffusion equation with the presence of convection by the variable velocity $u(x,t)$ and diffusion through the diffusion coefficient ϵ, see (22). We denote the diffusion coefficient by ϵ to emphasise that, according to our dimensional analysis, it has a small value. The temperature equation is then mostly of a convective nature and therefore close to hyperbolic.

To complete the system of equations, we introduce boundary and initial conditions. We only need one boundary condition for equation (23): velocity at the hot end $u_H(t)$. To find the velocity at the hot end we consider the volume flow through the orifice. From [4] the volume flow in a linear approximation is given by

$$\dot{V}_H(t) = -C_{or}(p_t(t) - p_b(t)), \tag{25}$$

where $p_t(t)$ is the tube pressure, $p_b(t)$ is the buffer pressure, C_{or} is the flow conductance of the orifice. The velocity is then given by:

$$u(0,t) = u_H(t) = -\frac{C_{or}}{A_t}(p_t(t) - p_b(t)), \tag{26}$$

where A_t the cross-sectional area of the tube. Special care has to be taken in determining the buffer pressure, such that the net mass flow over the hot end is zero. The derivation of the time-dependent buffer pressure is outlined in Appendix A. We perform the non-dimensionalisation of equation (26) just as in Section 3.2, by

taking $p_t(t) = p_0 + \bar{p}\hat{p}(t)$ and $p_b(t) = p_0 + \bar{p}\hat{p}_b(t)$. In dimensionless form (hats are omitted) the boundary condition for the velocity is

$$u_H(t) = -\mathcal{C}(p(t) - p_b(t)), \tag{27}$$

$$\mathcal{C} = \frac{C_{or}}{A_t} \frac{\bar{p}}{\bar{u}}, \tag{28}$$

where $\bar{p}$ and $\bar{u}$ are typical values for pressure and velocity. We assume constant temperature at the boundaries:

$$T(0,t) = T_H \quad , \quad T(L,t) = T_C. \tag{29}$$

As for the initial conditions, we only have to specify initial condition for the temperature:

$$T(x,0) = T^0(x). \tag{30}$$

4 Numerical solution

To solve the problem numerically, the governing partial differential equations (23)-(24) are discretised in space and time. We introduce computational grids $\{x_j = jh, j = 0, ..., N_x, h = \hat{L}/N_x\}$ and $\{t^n = n\tau^n, n = 0, ..., N_t\}$. Denote by u_j^n the velocity and by T_j^n the temperature at the grid point (x_j, t^n). We use the following formulae for the velocity computation:

$$
\begin{aligned}
u_j^n &= u_{j-1}^n + \frac{\epsilon}{h}(T_{j-1}^n - 2T_j^n + T_{j+1}^n) + hs_1(t^n) && j = 1, ..., N_x - 1, \\
u_{N_x}^n &= u_{N_x-1}^n + \frac{\epsilon}{h}(T_{N_x}^n - 2T_{N_x-1}^n + T_{N_x-2}^n) + hs_1(t^n) && j = N_x, \\
u_0^n &= u_H^n && j = 0,
\end{aligned}
\tag{31}
$$

for every time level $n = 0, 1, 2, 3, ...$ with u_H given by (27).

To solve the convection-dominated temperature equation we choose the following approach:

(i) *Convection.* Sharp resolution of discontinuities without excessive smearing: explicit time discretisation and a high-resolution scheme.

(ii) *Diffusion.* Explicit schemes lead to stability conditions of the type $\tau = O(h)$ for the convection term and $\tau = O(h^2)$ for the diffusion term. The last condition is too severe. One of the possibilities to avoid this restriction is to discretise the diffusion term implicitly.

The approximation of the convection term depends on the velocity sign, indicating the flow direction. If $u_j^n > 0$, we use the following scheme for the temperature equation:

$$
\begin{aligned}
T_j^{n+1} = T_j^n &+ \epsilon\tau^n T_j^n \frac{T_{j-1}^{n+1} - 2T_j^{n+1} + T_{j+1}^{n+1}}{h^2} + \tau^n s_2(t^{n+1})T_j^{n+1} \\
&- c_j^n \left(1 + \frac{1}{2}(1 - c_j^n)\left(\frac{\Phi_{j+\frac{1}{2}}^n}{r_{j+\frac{1}{2}}^n} - \Phi_{j-\frac{1}{2}}^n\right)\right)(T_j^n - T_{j-1}^n) \\
&j = 1, ..., N_x - 1, \quad n = 0, ..., N_t - 1.
\end{aligned}
\tag{32}
$$

If $u_j^n < 0$, then

$$
\begin{aligned}
T_j^{n+1} = T_j^n &+ \epsilon\tau^n T_j^n \frac{T_{j-1}^{n+1} - 2T_j^{n+1} + T_{j+1}^{n+1}}{h^2} + \tau^n s_2(t^{n+1})T_j^{n+1} \\
&- c_j^n \left(1 - \frac{1}{2}(1 + c_j^n)\left(\Phi_{j+\frac{1}{2}}^n - \frac{\Phi_{j-\frac{1}{2}}^n}{r_{j-\frac{1}{2}}^n}\right)\right)(T_{j+1}^n - T_j^n) \\
&j = 1, ..., N_x - 1, \quad n = 0, ..., N_t - 1,
\end{aligned}
\tag{33}
$$

where c_j^n is Courant number, $c_j^n = \tau^n u_j^n / h$. The ratio $r_{j+\frac{1}{2}}^n$ is defined by

$$r_{j+\frac{1}{2}}^n = \begin{cases} \dfrac{T_j^n - T_{j-1}^n}{T_{j+1}^n - T_{j'}^n} & \text{if} \quad u_j^n > 0, \\[3mm] \dfrac{T_{j+2}^n - T_{j+1}^n}{T_{j+1}^n - T_j^n} & \text{if} \quad u_j^n < 0. \end{cases} \tag{34}$$

$\Phi_{j+\frac{1}{2}}^n = \Phi(r_{j+\frac{1}{2}}^n)$ is the flux limiter. We have chosen a smooth van Leer limiter

$$\Phi(r) = \frac{r + |r|}{1 + |r|}. \tag{35}$$

For $r \le 0$ the limiter function $\Phi(r) = 0$. This means that, in the vicinity of extrema, where $r_{j+\frac{1}{2}}^n < 0$, the high resolution schemes (32) and (33) reduce to upwind schemes. If the CFL (Courant-Friedrichs-Lewy) stability condition $|c_j^n| \le 1$ or, equivalently,

$$\tau^n \le h / \max_j |u_j^n| \tag{36}$$

is satisfied, both schemes are second-order accurate in space away from discontinuities and first-order accurate in time, see [11].

The algorithm for numerical solution can be summarized as follows. Assume the initial temperature T_j^0 and velocity u_j^0 are given. At the beginning of each time step $n + 1$:

(1) Estimate $\max_j |u_j^n|$ at the previous time level and define τ^n, according to the CFL condition (36).

(2) Compute the temperature T_j^{n+1} from (32) if $u_j^n > 0$ or from (33) if $u_j^n < 0$, using T_j^n and u_j^n.

(3) Compute the velocity u_j^{n+1} via (31), using T_j^{n+1}.

The time integration proceeds until the system reaches the periodic steady state. We require that the difference in temperature between two consecutive cycles for all discretised points is less than a predefined tolerance.

5   Results and discussion

The parameter values for the typical single-inlet pulse tube we used in our simulation are given in Table 1. In our numerical experiments, we considered sinusoidal and step-function pressure variations shown in Figure 3. They correspond to the two different types of pulse-tube refrigerators: with Stirling-type compressor and with Gifford-McMahon-type compressor. However, a realistic pressure measurement can be accommodated to our model.
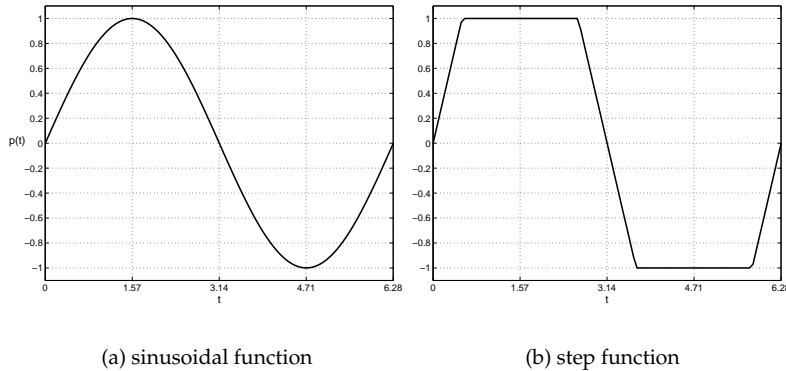

(a) sinusoidal function   (b) step function

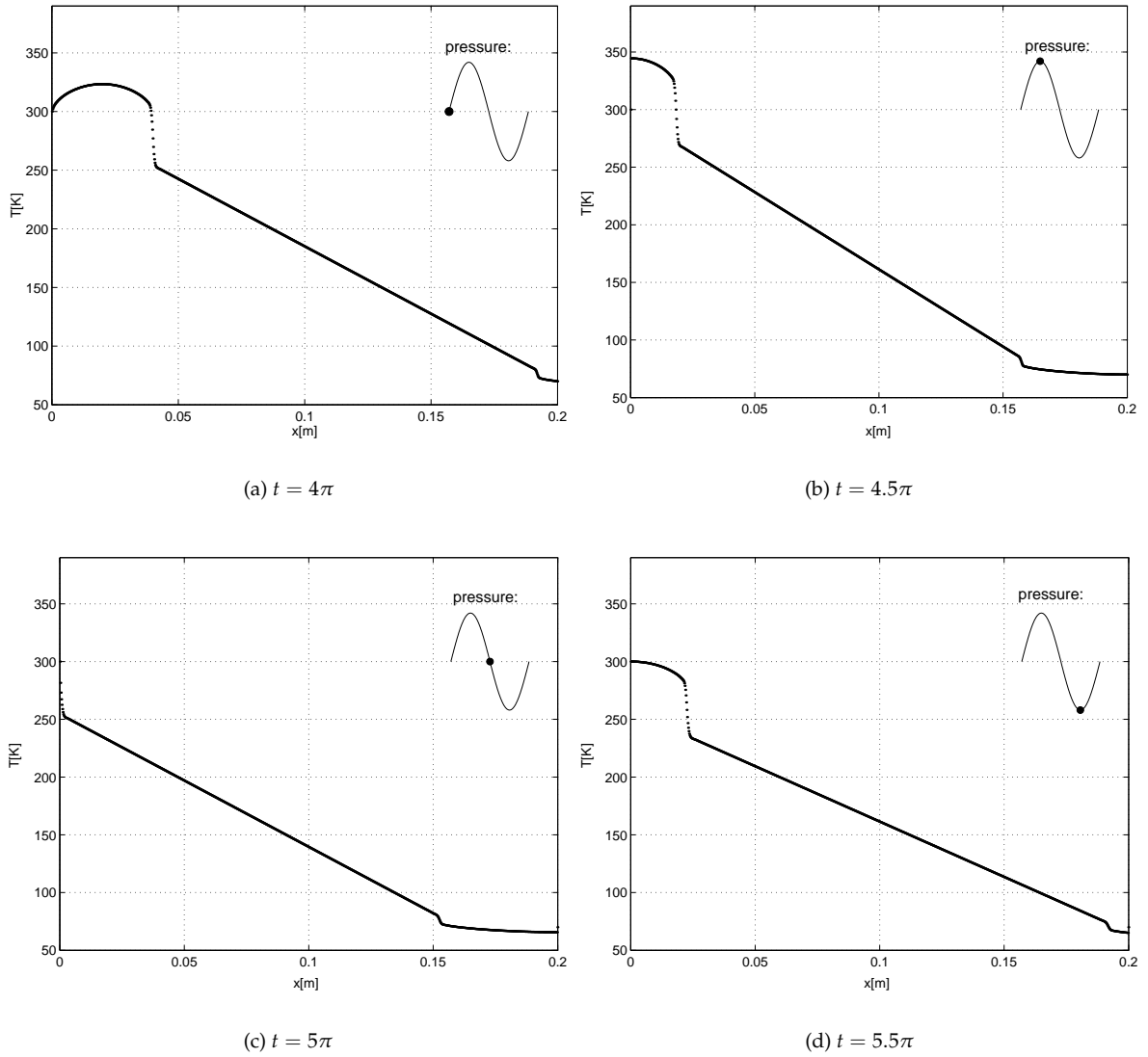Figure 3: Dimensionless pressure variation used in simulation.

Figure 4: Temperature profiles for the diffrerent parts of the pressure cycle ($h = 0.015$).

5.1 Temperature dynamics

Our model allows us to study the temperature dynamics in the tube.

In Figure 4 temperature profiles are depictured at times $t = 4\pi, 4.5\pi, 5\pi$ and 5.5π, which correspond to the different parts of the pressure cycle: 4π - pressure increases, 4.5π - maximum pressure, 5π - pressure decreases, 5.5π - minimum pressure. We used a sinusoidal pressure variation, boundary conditions $T_H = 300K$, $T_C = 70K$ and a linear temperature profile as initial condition. In Figure 5 temperature profiles are depictured on successively refined grids to show the convergence of our numerical solution. For comparison purpose we also plot the solution, obtained on the finest grid ($h = 0.015$) without flux-limiter.

Concerning the periodicity, for $h = 0.015$, we need 9 cycles to achieve the cycle-steady state with the tolerance $tol = 10^{-4}$. Figure 6 shows the temperature near the cold and hot ends after the system reached the steady state. For the sinusoidal pressure, we can compare the results of our calculations with the harmonic model described in [4] and with the three-dimensional results from [9]. The temperatures at the cold and warm ends for these two models are also depictured in Figure 6.

It is clear that all models show similar temperature dynamics. The numerical results differ slightly from the harmonic results, which are first-order approximations. In our simulation and in the three-dimensional simulation the initial temperature profile has been taken linear. We noticed that the temperature at both
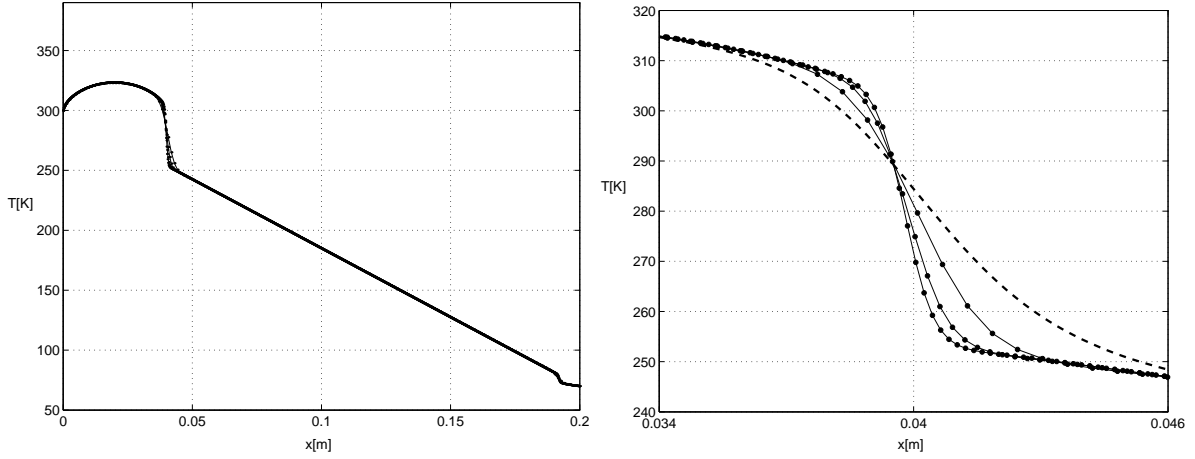
Figure 5: Temperature profiles at $t = 4\pi$ obtained on successively refined grids ($h = 0.05, 0.025, 0.015$). Dashed line - solution on the finest grid ($h = 0.015$), obtained without flux-limiter.

ends is sensitive to the initial profile in the first cycles where thermal conductivity has negligible effect. To study the influence of the initial conditions, we considered the following profiles (linear, exponential and step function):

$$T^0(x) = T_C(x/L) + T_H, \tag{37}$$

$$T^0(x) = T_H(T_C/T_H)^{x/L}, \tag{38}$$

$$T^0(x) = \begin{cases} T_H & \text{if} \quad x \leq L/2, \\ T_C & \text{if} \quad x > L/2. \end{cases} \tag{39}$$

The results of these simulations are shown in Figure 7. If the temperature near the boundaries is constant (step-function initial conditions), the overshoot in the temperature at both ends disappears.

Figure 8 shows the temperature at the cold and hot ends in case of the step-function pressure and with linear initial profile.

Using our model we can compute the position of the gas particles traveling with pressure oscillations inside the pulse tube. Therefore, we can follow the tracks of the gas particles in the pulse tube. Figure 9 shows the temperature of the gas versus position during one cycle for the two different pressure profiles. From these two figures it is clearly seen that the distance traveled by the gas particle and the temperature variation during the cycle are different at various pulse tube locations.
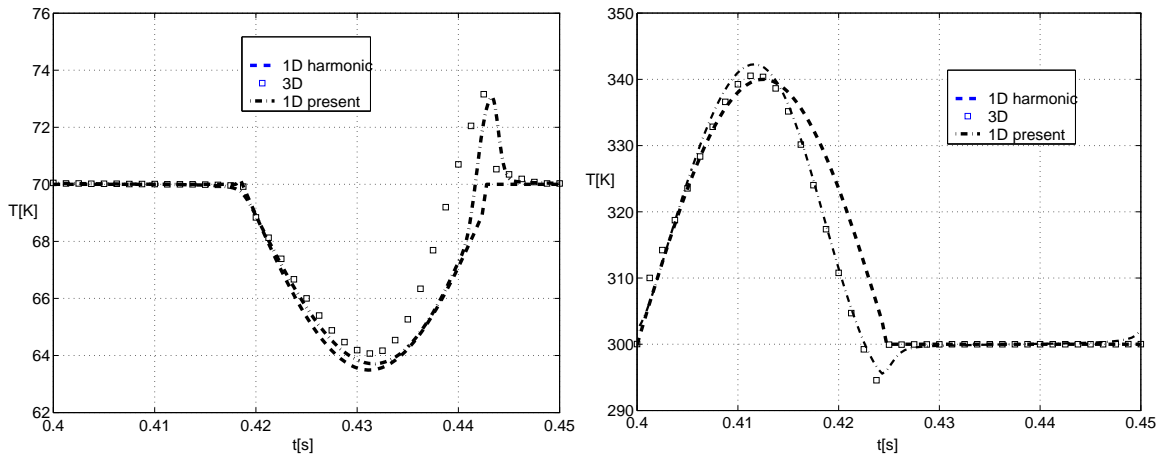

Figure 6: Temperature at cold and hot ends after 9 cycles with $h = 0.015$ (sinusoidal pressure).
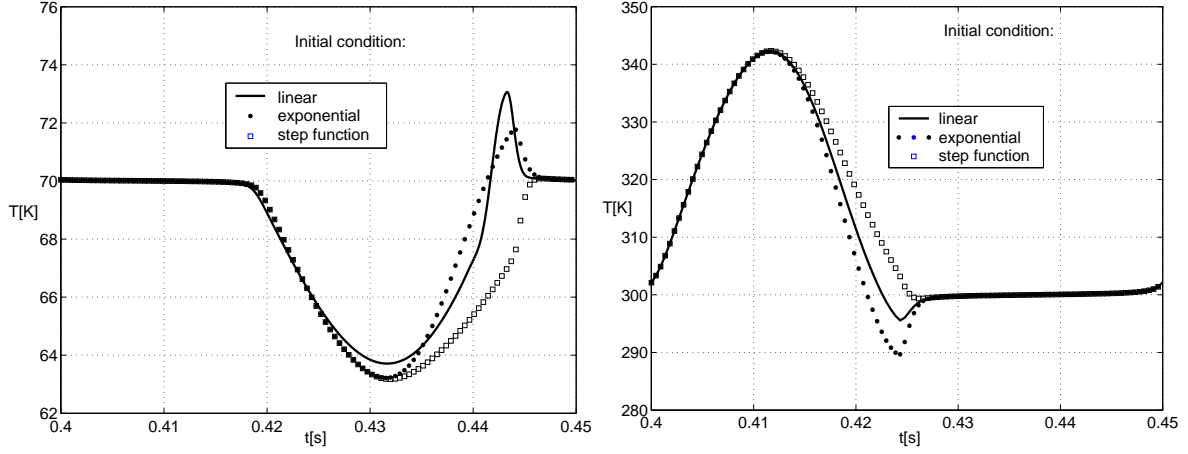
9

Figure 7: Temperature at cold and hot ends for the different initial conditions with $h = 0.015$ (sinusoidal pressure).
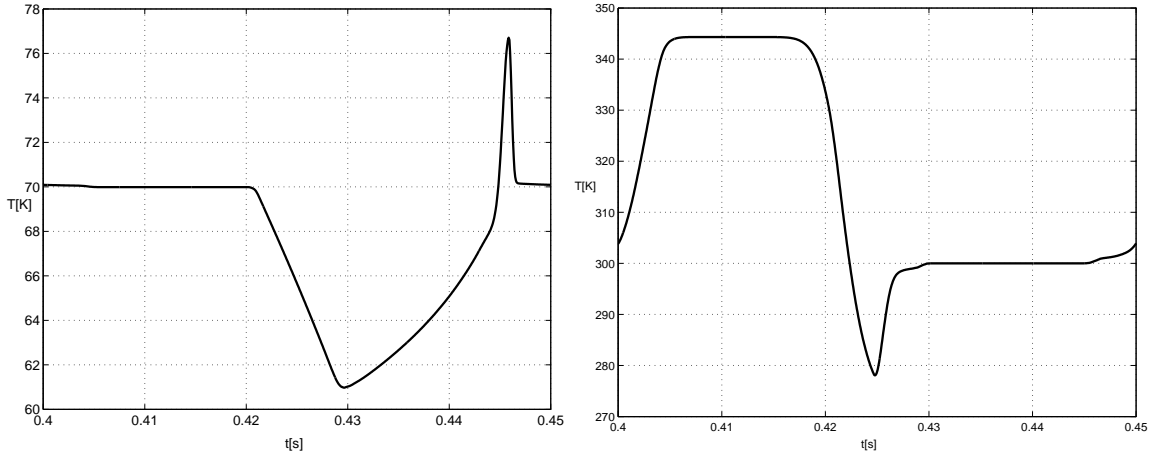

Figure 8: Temperature at cold and hot ends after 9 cycles with $h = 0.015$ (pressure - step function).

5.2   Mass flow rate and enthalpy flow

If velocity, temperature and density are known, we can compute the mass flow rate and the time-averaged enthalpy flow. The following formulas in dimensional form were used:

$$\dot{m} = A\rho u \,, \tag{40}$$

$$\dot{H} = \frac{c_p}{t_c} \int_0^{t_c} \dot{m}T \, dt, \tag{41}$$

where t_c is the cycle period.

Figure 10 shows the mass flow rate at the cold and hot ends for the sinusoidal and step-function pressure variation after 9 cycles. Note that the net mass flow should be close to zero. We want to point out that the mass flow is affected by the velocity boundary condition at the hot end. Even a small variation in this boundary condition can cause drift in the mass flow. If there is a net mass flow then the cycle-steady state can not be reached.

In Table 3, the values of the time-averaged enthalpy flow for different pressure profiles of the same amplitude are presented. These results show that the shape of the pressure oscillations influences the enthalpy flow in the tube and therefore affects the refrigeration power.
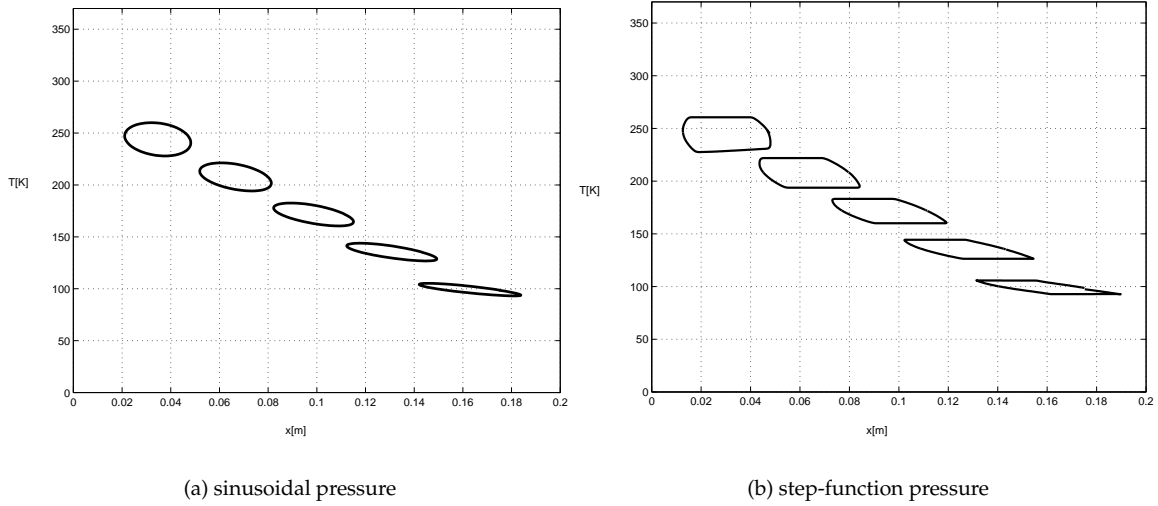
(a) sinusoidal pressure (b) step-function pressure

Figure 9: Tracks of gas particles for different pressure profiles.
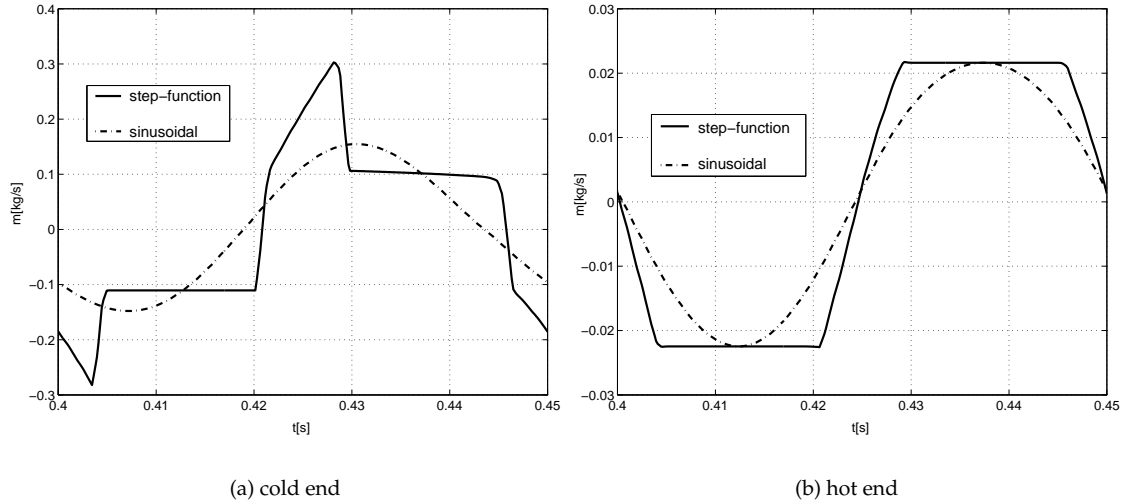

(a) cold end (b) hot end

Figure 10: Mass flow at cold and hot ends for two different pressure profiles with $h = 0.015$.

6 Conclusions

A one-dimensional model has been developed for simulating the oscillating gas flow in the tube section of a pulse-tube refrigerator. Conservation equations have been solved numerically. The momentum equation can be neglected as the pressure is considered to be a known function of time. Our analysis revealed that temperature in the tube is described by a convection-dominated equation. The governing equations have been solved with state-of-the-art flux-limiter schemes in an attempt to preserve the steep temperature gradients that occur in the tube. The tube's steady-state thermodynamic behaviour under sinusoidal and step-function pressure variations, and with different initial conditions, has been investigated. We validate our approach by comparing the results for sinusoidal pressure with the three-dimensional model and with the first-order harmonic model. The present method turns out to be more accurate and versatile than the first-order harmonic analysis and computationally less expensive than a three-dimensional simulation. With respect to refrigeration power our model can be used for calculating the optimal values of the system design parameters. In our future work we plan to apply a similar approach to the two-dimensional model. It will allow us to study many interesting phenomena, such as heat transfer between the gas and the tube walls, viscous effects and acoustic streaming.

Acknowledgments

Appendix A. Time dependent buffer pressure

This appendix outlines the derivation of the buffer pressure for the general form of the pressure oscillations. The expansion and compression in the buffer volume can be considered as adiabatic. In that case, according to the Poisson law, the volume flow through the orifice is

$$\frac{dV_H}{dt} = -\frac{c_v}{c_p}\frac{V_b}{p_b(t)}\frac{dp_b(t)}{dt}. \tag{A-1}$$

We also have (25)

$$\frac{dV_H}{dt} = -C_{or}(p_t(t) - p_b(t)). \tag{A-2}$$

Combining these two equations we obtain the following ordinary differential equation for the buffer pressure

$$\frac{dp_b}{dt} = \frac{C_{or}c_p}{V_b c_v}p_b(t)(p_t(t) - p_b(t)) \tag{A-3}$$

with initial condition $p_b(0) = p_0$. We perform non-dimensionalisation as in Section 3.2, taking $p_t(t) = p_0 + \bar{p}\hat{p}(t)$ and $p_b(t) = p_0 + \bar{p}\hat{p}_b(t)$. In dimensionless form equation (A-3) becomes

$$\begin{cases} \dfrac{d\hat{p}_b}{dt} = \mathcal{D}(\hat{p}_b(t) + \mathcal{A})(\hat{p}(t) - \hat{p}_b(t)) \\ \hat{p}_b(0) = 0 \end{cases} \tag{A-4}$$

where the dimensionless numbers $\mathcal{A}$ and $\mathcal{D}$ are defined as follows

$$\mathcal{A} = \frac{p_0}{\bar{p}}, \quad \mathcal{D} = \frac{C_{or}c_p}{V_b c_v}\frac{\bar{p}}{\omega}. \tag{A-5}$$

The nonlinear differential equation (A-4) is known as Ricatti's equation.

References

[1] E.I. Mikulin, A.A. Tarasov, M.P. Shkrebyonock, *Low temperature expansion pulse tubes*, Advances in Cryogenic Engineering 29 (1984), pp.629-637.

[2] M.Y. Xu, A.T.A.M. de Waele, Y.L. Ju, *A pulse tube refrigerator below 2K*, Cryogenics 39 (1999), pp.865-869.

[3] A.T.A.M. de Waele, P.P. Steijaert, J. Gijzen, *Thermodynamical aspects of pulse tubes*, Cryogenics 37 (1997), pp.313-324.

[4] A.T.A.M. de Waele, P.P. Steijaert, J. Gijzen, *Thermodynamical aspects of pulse tubes II*, Cryogenics 38 (1998), pp.329-335.

[5] C. Wang, P. Wu, Z. Chen, *Numerical modelling of an orifice pulse tube refrigerator*, Cryogenics 32 (1992), pp.785-790.

[6] Y. Hozumi, M. Murakami, *Numerical study of gas dynamics inside of a pulse tube refrigerator*, Advances in Cryogenic Engineering 45 (2000), pp.167-174.

[7] S.H. Baek, E.S. Jeong, S. Jeong, *Two-dimensional model for tapered pulse tubes. Part 1: theoretical modeling and net enthalpy flow*, Cryogenics 40 (2000), pp.379-385.

[8] S.H. Baek, E.S. Jeong, S. Jeong, *Two-dimensional model for tapered pulse tubes. Part 2: mass streaming and streaming-driven enthalpy flow loss*, Cryogenics 40 (2000), pp.387-392.

[9] D.W.J. Willems, J.A.M. Dam, *Three-dimensional pulse tube simulations*, Advances in Cryogenic Engineering 47 (2001), pp.934-941.

[10] W.R. Smith, *One-dimensional models for heat and mass transfer in pulse tube refrigerators*, Cryogenics 41 (2001), pp.573-582.

[11] R.M.M.Mattheij, S.W.Rienstra, J.H.M. ten Thije Boonkkamp, *Partial Differential Equations, Modelling, Analysis, Computing*, to appear in SIAM Press.

Symbol	Definition	Value
f	frequency	20 Hz
ω	angular frequency	125.66 s^{-1}
$\bar{\rho}$	gas density	4.7 kg m^{-3}
$\bar{u}$	gas velocity	1.5 m s^{-1}
$\bar{\mu}$	viscosity	2.0×10^{-5} Pa s
$\bar{k}_g$	gas thermal conductivity	1.58×10^{-1} W m^{-1} K^{-1}
c_p	gas specific heat capacity	5.2×10^3 J kg^{-1}K^{-1}
$\bar{p}$	pressure oscillation amplitude	5×10^5 Pa
p_0	average pressure	3×10^6 Pa
T_a	ambient temperature	300 K
R_m	specific gas constant	2.1×10^3 J kg^{-1}K^{-1}
A_t	cross-sectional area of tube	2×10^{-3} m^2
D	tube diameter	7×10^{-2} m
C_{or}	flow conductance of the orifice	10^{-8} m^3 Pa^{-1}s^{-1}
L	length of tube	0.2m
T_H	hot end temperature	300K
T_C	cold end temperature	70K
V_b	buffer volume	5×10^{-3} m^3

Table 1: Physical data for a typical single-inlet pulse tube (values at 300K)

Symbol	Definition	Typical Value
Re	$\bar{\rho}\bar{u}^2/\bar{\mu}\omega$	4×10^3
Ma	$\bar{u}/(\bar{p}/\bar{\rho})^{1/2}$	4.6×10^{-3}
Pr	$c_p\bar{\mu}/\bar{k}_g$	0.658
Pe	RePr	2.6×10^3
Ec	$\bar{u}^2/c_pT_a$	1.5×10^{-6}
1/Ma^2	$\bar{p}/\bar{\rho}\bar{u}^2$	4.7×10^4
1/Re	$\bar{\mu}\omega/\bar{\rho}\bar{u}^2$	2.5×10^{-4}
Ec/Ma^2	$\bar{p}/\bar{\rho}c_pT_a$	7×10^{-2}
1/Pe	$\bar{k}_g\omega/\bar{\rho}c_p\bar{u}^2$	3.6×10^{-4}
$\mathcal{A}$	$p_0/\bar{p}$	6
$\mathcal{B}$	$\bar{p}/\bar{\rho}R_mT_a$	0.17
$\mathcal{C}$	$C_{or}\bar{p}/A_t\bar{u}$	1.67
$\mathcal{D}$	$C_{or}c_p\bar{p}/V_Bc_v\omega$	$1/24\pi$

Table 2: Dimensionless parameters for a typical single-inlet pulse tube

	harmonic	step function
cold end	1258W	1969W
warm end	1259W	1963W

Table 3: Time-averaged results for enthalpy flow $\dot{H}$ with $h = 0.015$.

Nomenclature

A_t	cross-sectional area of tube		*Greek letters*	
C_{or}	flow conductance of the orifice		ρ	gas density
c_p	constant pressure heat capacity		μ	viscosity
c_v	constant volume heat capacity		ω	angular frequency
D	tube diameter			
$\dot{H}$	enthalpy flow		*Dimensionless*	
k_g	gas thermal conductivity		Ec	Eckert number
L	tube length		Ma	Mach number
$\dot{m}$	mass flow		Pe	Peclet number
p_0	average pressure		Pr	Prandtl number
$\bar{p}$	pressure oscillation amplitude		Re	Reynolds number
p_b	buffer pressure		$\mathcal{A}$	pressure ratio
p_t	tube pressure		$\mathcal{B}$	constant
$\dot{Q}_H$	heat extracted at hot end		$\mathcal{C}$	constant
$\dot{Q}_C$	heat loaded at cold end		$\mathcal{D}$	constant
R_m	specific gas constant			
T	gas temperature			
T_a	ambient temperature			
T_C	cold end temperature			
T_H	hot end temperature			
t_c	period of one cycle			
u	gas velocity			
V_b	buffer volume			
$\dot{V}_H$	volume flow			